

Numerical Study on Discharge Characteristics of a Line-Shaped Microwave Plasma with a Rectangular Slotted Waveguide

Akihiro TSUJI, Yasuyoshi YASAKA, Hiromasa TAKENO

Electrical and Electric Engineering, Graduate School of Engineering, Kobe University

Takayuki FUKASAWA, Shuitsu FUJII

Adtec Plasma Technology Co. Ltd.

(Received: 1 September 2008 / Accepted: 18 December 2008)

A three-dimensional fluid simulation code has been developed for investigating characteristics of wave propagations and plasma productions in a line-shaped plasma device. In numerical analyses of the wave propagations, it is shown that distributions of power absorption depending on the wave propagations change by adjusting a width of a waveguide and an insertion depth of the plasma to the waveguide and both spatial and plasma resonances arise near the plasma surface. In addition, the simulation in a certain condition shows that the device can produce the plasma with good uniformity in the longitudinal direction. These results given by computational studies theoretically support to explain the characteristics of the line-shaped plasma produced in the device and indicate that the distributions of the wave propagations and the plasmas can be controlled by adjusting the width of the waveguide and/or the insertion depth of the plasma to the waveguide.

Keywords: microwave-excited plasma, spatial resonance, plasma resonance, numerical calculation, three-dimensional fluid simulation

1. Introduction

Plasma processing is used in microfabrications including an etching, a film formation and a surface modification and it supports current semiconductor manufacturing. Recently the plasmas which fulfill large area, good uniformity, high electron density and low electron temperature in a wide range of gas pressure are required for an improvement of the performance. The plasma devices with various production mechanisms such as inductively-coupled plasmas (ICPs) [1-3], capacitively-coupled plasmas (CCPs) [4, 5], electron cyclotron resonance (ECR) plasmas [6, 7] and so on have been developed and investigated in the past. Each device has advantages and disadvantages. Microwave-excited plasmas without external magnetic fields have the advantages that the plasmas have high electron density and low electron temperature in general [8] and the plasmas with the diameter larger than that of the antennas can be produced by using the electromagnetic fields propagating on the plasma surface or in the plasma. On the other hand, they have disadvantages that it is not easy to control the uniformity of the plasma parameters due to mode jumps of surface wave eigenmodes [9].

The researches of the microwave-excited plasmas have a long history. The microwave-excited long plasma columns reported by Moisan *et al.* [10-12] and Kato *et al.* [13] were used for a surface modification at a local area and the light source of a laser. After a while planar plasmas suitable for the large area processing could be

produced by Komachi *et al.* [14] and later by other investigators [15-19] by using various structures and excitation method. The large planar plasmas are expected to be used for etching and deposition processes on large wafers of next generation.

The large-area plasma processing can also be accomplished by scanning the line-shaped plasma over the area. One of the devices based on such concept, the line plasma device [20], consists of a rectangular waveguide with a long and thin slot on an E-surface, a quartz discharge tube which is partly inserted in the slot and has a U-shaped cross section with an opening opposite to the waveguide, and a diffusion chamber connected to the opening. This device is similar to the devices reported by Ohl [21] and Pollak *et al.* [22] in the sense that the microwaves propagate in a waveguide structure to form a distributed power source for plasma production along the long column. The line plasma device, however, has advantages over these devices such that the wave profile in the waveguide is adjustable for the control of plasma uniformity along the column. The wave profile can be adjusted by the width of the waveguide and/or the insertion depth of the plasma because the wavelength of the electromagnetic fields propagating in the rectangular waveguide depends on the size and the medium. Moreover, the device has the simple structure without an interface waveguide and some coupling elements. In this device, the experiments and the numerical analyses have shown that the wave propagation can be controlled by

author's e-mail : a.tsuji@stu.kobe-u.ac.jp

changing the width of the waveguide and/or an insertion depth of the plasma and the line-shaped plasma can be produced [20, 23].

We have developed a three-dimensional (3D) fluid simulation code of the line-shaped plasma and performed the numerical analyses and the simulations for explaining some physical mechanisms. According to authors' knowledge, the 3D fluid simulations for such devices have not been reported. In this paper, we describe the characteristics of the wave propagations and plasma productions obtained from the results.

2. Simulation Procedure and Basic Equations

In the fluid simulation for the line-shaped microwave plasmas, wave propagations, power absorptions, plasma transports and gas phase chemical reactions are self-consistently solved as shown in Fig. 1 [23, 24]. The wave propagations in the rectangular waveguide, the quartz discharge tube and the plasma chamber are calculated by the finite-difference time-domain (FDTD) scheme [24]. The Basic equations in the FDTD scheme are Faraday's law of induction;

$$\nabla \times \mathbf{E} = -\mu_0 \frac{\partial \mathbf{H}}{\partial t} \quad (1)$$

and Ampere's circuital law;

$$\nabla \times \mathbf{H} = \mathbf{J} + \varepsilon \varepsilon_0 \frac{\partial \mathbf{E}}{\partial t}, \quad (2)$$

where \mathbf{E} , \mathbf{H} , \mathbf{J} , ε , ε_0 and μ_0 represent electric fields, magnetic fields, current density, relative permittivity, permittivity and permeability in vacuum, respectively. In the plasma, the equation of the current density;

$$\mathbf{J} \cong -en_e \mathbf{v}_e \quad (3)$$

and the equation of motion for electrons;

$$m_e \frac{\partial \mathbf{v}_e}{\partial t} = -e\mathbf{E} - m_e \nu_m \mathbf{v}_e \quad (4)$$

are used in addition to Eqs. (1) and (2), where e , n_e , \mathbf{v}_e , m_e and ν_m represent the electron charge, electron density, velocity of electron, the electron mass and momentum transfer collision frequency, respectively. In the analytic space, a metallic surface and an open region exist as boundaries. The boundary condition of the metallic surface is that the tangential component of the electric fields equals to zero and Mur's absorbing boundary condition (ABC) of 2nd order is used as that of the open region. The energy transfer from the waves to the plasma assumes that the joule heating of the electrons;

$$P_{\text{abs}} = \frac{1}{T} \int_t^{t+T} \mathbf{J} \cdot \mathbf{E} dt \quad (5)$$

is the main energy transfer mechanism, where P_{abs} and T represent the power absorbed to the electrons and a time cycle of the microwave, respectively. In the plasma transports, the equation of continuity;

$$\frac{\partial n_e}{\partial t} + \nabla \cdot \mathbf{\Gamma}_e = \left(\sum_i \nu_{\text{ion},i} - \sum_i \nu_{\text{rec},i} \right) n_e \quad (6)$$

and the energy conservation equation;

$$\begin{aligned} & \frac{\partial}{\partial t} \left(\frac{3}{2} n_e k_B T_e \right) + \nabla \cdot \left(\frac{5}{2} k_B T_e \mathbf{\Gamma}_e + \kappa \nabla k_B T_e \right) \\ & = P_{\text{abs}} - \left(\frac{3m_e}{M} \nu_m k_B T_e + \sum_i \sum_j e V_{ij} \langle \sigma_{ij} v_e \rangle n_i \right) n_e \end{aligned} \quad (7)$$

are used, where $\mathbf{\Gamma}$, ν_{ions} , ν_{rec} , k_B , T_e , κ , V_{ij} and σ_{ij} represent the particle flux, the ionization frequency, the recombination frequency, Boltzmann constant, electron temperature in K, thermal conductivity, the threshold energy in eV and the collision cross-section of the j -th reaction for an electron and i -th particle, respectively. Bohm condition at a sheath edge is used as the boundary condition on the metallic surface [25]. In the gas phase chemical reactions, the rate equation;

$$\begin{aligned} \frac{\partial n_k}{\partial t} + \nabla \cdot \mathbf{\Gamma}_k &= \sum_i \langle \sigma_{ik} v_e \rangle n_e n_i + \sum_i \sum_j R_{ijk} n_i n_j \\ &- \left(\sum_i \langle \sigma_{ki} v_e \rangle n_e + \sum_i \sum_j R_{kij} n_i \right) n_k \end{aligned} \quad (8)$$

is used, where n_k and R_{ijk} represent a density of k -th neutral particle and the rate constant of the reaction in which i -th particle and j -th particle yield k -th particle, respectively. On the metallic surface, the sticking of particles is considered [22]. The time step of each calculation is defined by Courant condition.

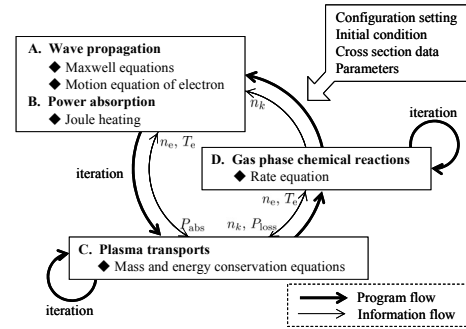


Fig.1 Simulation procedure. The simulation code time-developmentally implements the calculations of the wave propagations, the power absorptions, the plasma transports and the gas phase chemical reactions after loading some external files.

3. Calculation Model of a Line-Shaped Plasma

A calculation model of the line-shaped plasma is composed of the rectangular slotted waveguide, the quartz discharge tube and the plasma chamber as shown in Fig. 2. Two pairs of a normal and a tapered waveguides are set at both sides of the narrow waveguide. Microwave sources driven at $\omega/2\pi = 2.45$ GHz are set on a single side or both sides of the end faces of the normal waveguides and form the electromagnetic fields of TE₁₀ mode in the normal rectangular waveguides. In the single microwave source only, the ABC is used on the other side. The x -directional width of the normal waveguide is 110 mm supposing a rectangular waveguide of WRJ-2 type and that of the narrow waveguide, a , is varied near 62 mm. An insertion depth, d_i , of the plasma to lower surface of the narrow waveguide is varied from -3 to 3 mm. The size of the chamber is 6, 3 and 40 cm for x -, y - and z -directions, respectively. Note that the size of the

calculation model is smaller than that of the device used in the experiments because the calculation cost depends on the size of the analytic space. The cell size used in the all calculations is 1, 1 and 5 mm for x -, y - and z -directions, respectively.

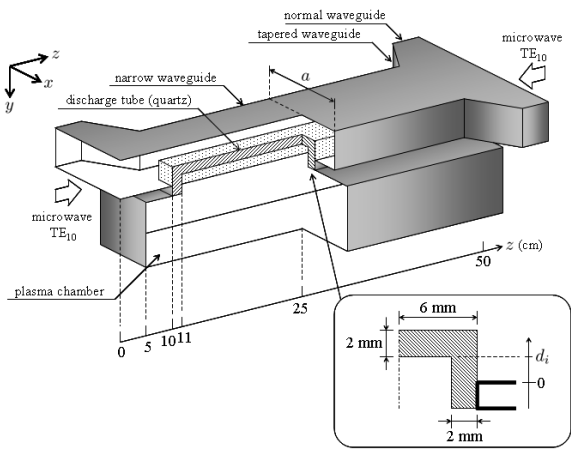


Fig.2 The calculation model of the line-shaped plasma device. It is composed of the rectangular slotted waveguide, the quartz discharge tube and the plasma chamber.

4. Results and Discussions

4.1 Numerical Analyses of Wave Propagations

The comparatively uniform distribution of the power absorption from the electric fields to the electrons is required for producing the line-shaped plasmas with good uniformity in the z -direction because the plasmas are produced by the electric fields radiated from the slot. Therefore, it is important to investigate the distribution of the power absorption in the case that the conditions such as the width of the waveguide, the insertion depth and the plasma parameters are changed. In addition, a spatial resonance at the plasma-quartz interface and/or a plasma resonance in the plasma probably arise. In this subsection, the distributions of the power absorption and the electric field intensity are investigated by the numerical analyses.

We have calculated the electric fields in the case without the plasma by using Eqs. (1) and (2), where $\mathbf{J} = 0$. Figure 3 shows the spatial distribution of the electric field intensity, where the conditions are $a = 62$ mm and $d_i = 1$ mm. The microwave propagates in the waveguide and the discharge tube and is radiated downwards from the slot. In this case, the electric field intensity in the narrow waveguide is stronger than that in the other space. On the other hand, the electric field intensity in the plasma chamber becomes strong just under the discharge tube as shown in Fig. 3. Therefore, it is expected that the plasma in the device is mainly produced in this region.

We have calculated the electric fields in the case that the plasma is filled with the uniform plasma by using Eqs. (1) to (4). In this calculation, the microwave source is set at the single side of $z = 0$. The z -directional distribution of the power absorption $P_{\text{abs}}(z)$ on the plasma-quartz surface is

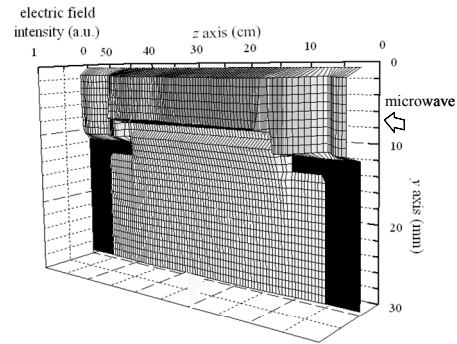
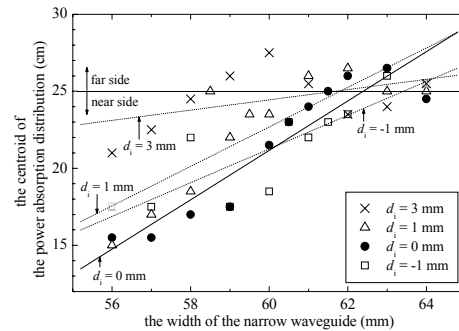


Fig. 3 The spatial distribution of the electric field intensity in the case without the plasma.

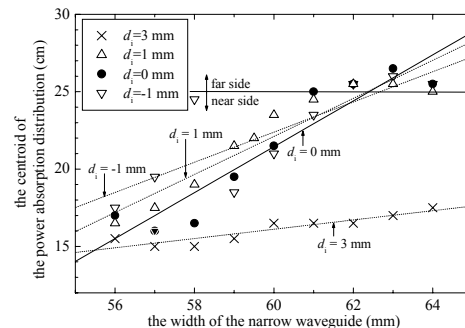
given by the results and Eq. (5). The centroid, g , given by

$$\int_{z_1}^{z_2} (g - z) P_{\text{abs}}(z) dz = 0 \quad (9)$$

is used as the index to characterize it, where $z_1 = 11$ cm and $z_2 = 39$ cm. Figure 4 shows the centroid of the power absorption distribution for some patterns of the width of the narrow waveguide and the insertion depth. Note that it is difficult to produce the line-shaped plasmas as the centroid is smaller than $z = 25$ cm because the electric fields hardly propagate through the waveguide to the other side. The results show that the electric fields hardly propagate through the waveguide to the other side as the width of the waveguide is shorter than a certain width in various insertion depths in the case of low electron density, 10^{10} cm^{-3} , as shown in Fig. 4(a) or the insertion depth is too



(a) $n_e = 10^{10} \text{ cm}^{-3}$



(b) $n_e = 10^{12} \text{ cm}^{-3}$

Fig. 4 The centroid of the power absorption distribution for some patterns of the width of the narrow waveguide and the insertion depth. Solid and dotted lines are the approximate lines given by the linear fitting for the results of each insertion depth.

large in the case of high electron density, 10^{12} cm^{-3} , as shown in Fig. 4(b). Therefore, the distribution of the power absorption is determined by the width of the waveguide and the insertion depth and the insertion depth must be kept shallow to produce the line-shaped plasmas with high electron density.

The spatial resonance arises at a certain condition of the device structure and the plasma parameters. Figure 5 shows the ratio of the electric field intensity obtained by the numerical analysis for uniform plasmas with a certain plasma density, where the ratio is the electric field intensity at the plasma-quartz interface divided by that in the waveguide. In the analyses, we use $a = 62 \text{ mm}$, $v_m/\omega = 0$ and $d_i = -1, 0$ and 1 mm . The electric field ratio has some peaks in the specific range of the electron density, and the maximum value is about 11 at $n_e = 4 \times 10^{11} \text{ cm}^{-3}$ in the case of $d_i = 1 \text{ mm}$. The peaks mean the existence of the spatial resonance. Figure 6 shows the spatial distribution of the electric field intensity normalized by the maximum value, where the plasma in the chamber has uniform electron density of $4 \times 10^{11} \text{ cm}^{-3}$. From the result, we obtain that the electric field intensity has some peaks on the plasma-quartz interface and is much stronger than that in the waveguide or the discharge tube. Therefore, we anticipate that the spatial resonance on the plasma-quartz interface arise in the real device.

The plasma resonance which is a field enhancement phenomenon at the position of a local plasma resonance arises at a specific electron density of about $7.4 \times 10^{10} \text{ cm}^{-3}$ in the case of $\omega/2\pi = 2.45 \text{ GHz}$ [25, 26]. Figure 7 shows

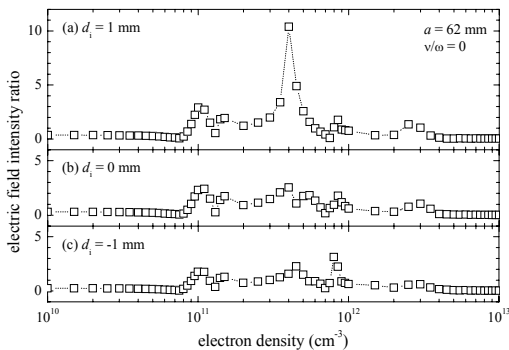


Fig. 5 The ratio of the electric field intensity given by the numerical analyses for uniform plasmas with a certain plasma density, where the ratio is the electric field intensity at the plasma-quartz interface divided by that in the waveguide.

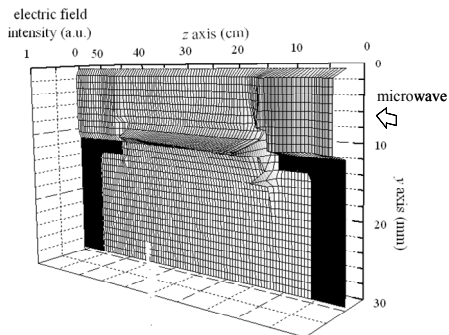


Fig. 6 The spatial distribution of the electric field intensity in the device, where the plasma density in the chamber is uniform and equals to $4 \times 10^{11} \text{ cm}^{-3}$. The electric field intensity has some peaks on the plasma-quartz interface.

the spatial distribution of the electric field intensity normalized by the maximum value, where the plasma in the chamber has density gradient. In this analysis, the electron density smoothly increases up to $5 \times 10^{11} \text{ cm}^{-3}$ toward both y - and z -directions and the other conditions are the same as those of the analyses for the spatial resonance. As a result, we obtain that the electric field intensity has some peaks in the plasma region and the electron density at the peaks is about $7.4 \times 10^{10} \text{ cm}^{-3}$. Therefore, we anticipate that the plasma resonance at the position with the specific electron density arises in the real device.

In the viewpoint of the wave propagations, this device requires that electric fields can propagate through the waveguide to the other side for the line-shaped plasma production. This requirement is solved by adjusting the width of the waveguide and/or the insertion depth of the plasma to the waveguide. The distribution of the plasmas, however, is not decided by the electric field distribution in the waveguide only because the spatial and plasma resonances arise in the plasma region near the discharge tube. The plasmas using the spatial resonance such as surface waves plasmas (SWPs) have a potential to produce the plasmas with high electron density because the electric fields enhanced by the spatial resonance locally heats the plasmas on the plasma-quartz interface. In addition, such plasmas probably carry the nonuniformity due to a surface wave eigenmode. Therefore, the spatial resonance must be suppressed for producing the line-shaped plasmas unless the z -directional wavelength of the electric fields enhanced by the excitation of the surface wave eigenmode is longer than the chamber size. A countermeasure against the spatial resonance is to adjust the insertion depth because the resonance condition depends on the device structure except the plasma parameters as shown in Fig. 5. The plasma resonance generally arises at the position of the specific electron density in nonuniform plasmas with the density gradient. The distribution of the electric fields enhanced by the plasma resonance nearly depends on the electric fields radiated from the slot. From this reason, the key parameters by which the distribution of the plasma parameters is mainly decided are the width of the waveguide and the insertion depth.

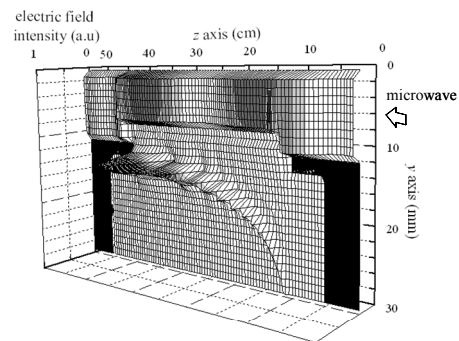


Fig. 7 The spatial distribution of the electric field intensity in the device, where the plasma in the chamber has density gradient. The electric field intensity has some peaks in the plasma region.

4.2 Fluid Simulations

We perform the fluid simulations of the line-shaped plasmas for investigating the production mechanism. The microwave is excited from both sides of the waveguide and the phase difference between two microwave sources is zero. The total power absorbed to the electrons, P_{total} , is calculated by the global electric fields of steady state, where the electric fields are given after the calculations of transient state for 10 cycles of the microwave. It is assumed that the chamber is uniformly filled with Ar gas at gas pressure of 200 mTorr. Excitation, ionization and recombination in Ar plasma are considered in the gas phase chemical reactions [24]. The electromagnetic fields are calculated in the whole region to consider the interferential effect. In the calculations of the plasma transports and the gas phase chemical reaction, quarter computational domain is used because the distribution of the power absorption has symmetrical relations in the x - and the z -directions. The simulations are performed until the simulation time of 1 msec. Note that the steady distributions of the plasma parameters are approximately formed by this time.

Figure 8 shows the distribution of the plasma parameters given by the simulation in the case of $a = 62$ mm, $d_i = -2$ mm and $P_{total} = 100$ W. As a result, it is observed that the plasma parameters at some distance from the discharge tube are comparatively uniform distribution in the z -direction although they have some peaks near the plasma quartz interface. The maximum values of the electron density and temperature are 1.1×10^{13} cm^{-3} and 3.5 eV, respectively, and are located near the z -directional both edges of the plasma-quartz interface. The region with higher plasma parameters is formed near the plasma surface due to the electric fields enhanced by the spatial and/or the plasma resonances. Therefore, it means that the plasmas in the device are efficiently produced not only by using the electric field radiated from the slot but also by exciting the resonance phenomenon near the plasma surface.

Figure 9 shows the z -directional distribution of the electron density in the case of $d_i = 2, 0$ and -2 mm, where fixed parameters are $P_{total} = 100$ W and $a = 62$ mm. As a result, it is observed that the distributions of the electron density become comparatively uniform at $y = 20$ mm as shown in Fig. 9 (b), although they have a peak near the edge of the plasma-quartz interface at $y = 10$ mm as shown in Fig. 9 (a). In particular, the uniformity in the range of $z = 15$ to 25 cm at $y = 20$ mm in the case of $d_i = -2$ mm is better than those in the case of $d_i = 2$ and 0 mm. It means that the distribution of the plasma parameters strongly depends on the insertion depth and the peak of the plasma parameter at the edge of the plasma-quartz interface is clearly observed as the plasma is deeply inserted to the waveguide. Therefore, the production of the line-shaped plasmas with good uniformity of plasma

parameters in the z -direction requires the suitable control of the width of the waveguide and the insertion depth of the plasma to the waveguide.

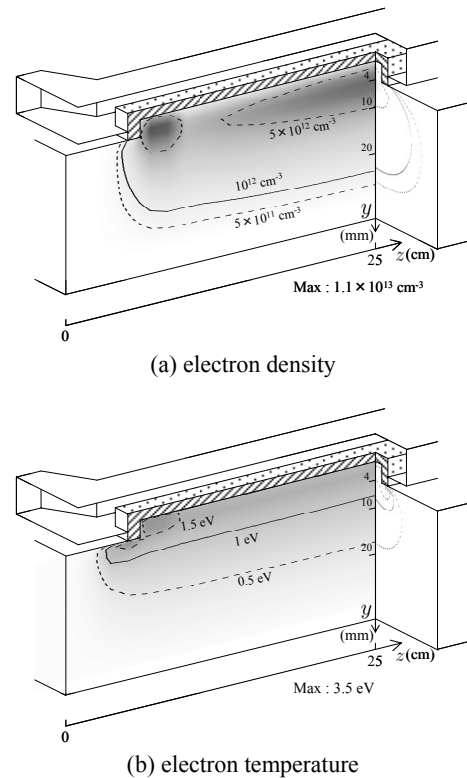


Fig. 8 The distribution of the plasma parameters given by the simulation in the case of $a = 62$ mm, $d_i = -2$ mm and $P_{total} = 100$ W.

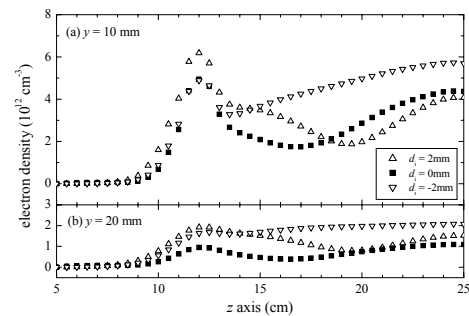


Fig.9 The z -directional distribution of electron density in the case of $d_i = 2, 0$ and -2 mm, where fixed parameters are $P_{total} = 100$ W and $a = 62$ mm.

5. Summary

In this study, we developed the 3D fluid simulation code for the line-shaped plasma device and investigated the characteristics of the wave propagations and the plasma productions. The principal results are summarized below.

The simulations show that the plasma with good uniformity in the z -direction can be produced although the peaks of the plasma parameters are observed at the local position. In addition, it also shows that the peaks are clearly observed as the plasma is deeply inserted to the

waveguide. It results from the fact that the electric fields hardly propagate through the waveguide as the plasma with high electron density is deeply inserted as shown in Fig. 4 (b). On the other hand, the numerical analyses show that the distribution of the power absorption can be controlled by selecting the suitable parameters as shown in Fig. 4. Therefore, the line-shaped plasma can be produced by controlling the external parameters. Moreover, both the spatial and the plasma resonances arise at the specific region as shown in Figs. 5 to 7. As a result, we indicate that the plasmas in the device are efficiently produced not only by using the electric fields radiated from the slot but also by exciting the resonance phenomenon near the plasma surface.

- [1] K. Kondo *et al.*, Appl. Phys. Lett. **65**(1), 31 (1994).
- [2] W. Z. Collison *et al.*, IEEE Trans. Plasma Sci. **24**(1), 135 (1996).
- [3] M. Tadokoro *et al.*, Phys. Rev. E **58**(6), 7823 (1998).
- [4] T. Kitajima *et al.*, J. Phys. D: Appl. Phys. **30**(12), 1783 (1997).
- [5] M. J. Kushner, J. Appl. Phys. **94**(3), 1436(2003).
- [6] S. Samukawa *et al.*, J. Vac. Sci. Technol. B **8**, 1192 (1990).
- [7] Y. Yasaka *et al.*, J. Appl. Phys. **72**(7), 2652 (1992).
- [8] M. Umeno *et al.*, Diamond and Related Materials **14**(11-12), 1973 (2005).
- [9] H. Sugai *et al.*, Plasma Sources Sci. Technol. **7**(2), 192 (1998).
- [10] M. Moisan *et al.*, IEEE Trans. Plasma Sci., **PS-3**, 55 (1975).
- [11] M. Moisan *et al.*, Can. J. Phys. **60**, 379 (1981).
- [12] M. Moisan *et al.*, J. Phys. D: Appl. Phys. **24**(7), 1025 (1991).
- [13] I. Kato *et al.*, J. Appl. Phys. **51**, 5312 (1980).
- [14] K. Komachi *et al.*, J. Microwave Power Electromagn. Energy **24**(3), 140 (1989).
- [15] Y. Yasaka *et al.*, Plasma Sources Sci. Technol. **8**(4), 530 (1999).
- [16] Y. Yasaka *et al.*, IEEE Trans. Plasma Sci. **32**(1), 101 (2004).
- [17] M. Nagatsu *et al.*, Appl. Phys. Lett. **87**(16), 161501 (2005).
- [18] H. Kousaka *et al.*, Vacuum **80**(7), 806 (2006).
- [19] A. Tsuji *et al.*, Surface and Coatings Technol. **202**(22-23), 5306(2008).
- [20] T. Fukasawa *et al.*, 20th Symp. Plasma Sci. for Materials, June 21-22, 77 (2007).
- [21] A. Ohl, J. Phys. IV **8**(P7), 83 (1998).
- [22] J. Pollak *et al.*, Plasma Sources Sci. Technol. **16**, 310 (2007).
- [23] A. Tsuji *et al.*, 25th Symp. Plasma Processing, Jan. 23-25, 209 (2008).
- [24] Y. Yasaka *et al.*, Jpn. J. Appl. Phys. **45**(10B), 8059 (2006).
- [25] A. Tsuji *et al.*, Thin Solid Films **516**(13), 4368 (2008).
- [26] M. Zethoff *et al.*, J. Phys. D: Appl. Phys. **25**(11), 1574 (1992).
- [27] Y. Yasaka *et al.*, Phys. Plasmas **7**(5), 1601 (2000).